Preprints of the 19th World Congress
The International Federation of Automatic Control
Cape Town, South Africa. August 24-29, 2014

Robust tracking control of 6-DOF parallel electrical manipulator in Joint-Task space with fast friction estimation ⋆

Renjian Hao * **Junzheng Wang** ** **Jiangbo Zhao** ***
Shoukun Wang ***

* *Beijing Institute of Technology, Beijing, China (e-mail: haorenjian@gmail.com).*
** *Beijing Institute of Technology, Beijing, China (e-mail: Wangjz@bit.edu.cn).*
*** *Beijing Institute of Technology, Beijing, China.*

Abstract: This paper presents a robust tracking controller equipped with a fast friction estimator for a 6-DOF parallel electrical manipulator in the joint-task space. Parallel manipulator control scheme mainly stems from two frameworks: the task space control and the joint space control. The former requires the system states obtained via costly direct measurements or time-consuming forward kinematics. The latter's performance is subject to the inaccurate dynamic model. To minimize their weaknesses, the joint-task space framework is constructed by transforming the dynamics on the task space into the joint space. With this transformation, the desired positional data are used to calculate the nominal value of dynamics. On the other hand, the friction property depends on the uncertain load condition due to the spiral drive way of the electrical cylinders. A fast friction estimator is then designed to estimate the uncertain friction fast and effectively. The robust control scheme is proposed based on the Lyapunov design method to guarantee a practical stability under uncertainties such as inertia, modeling errors, friction, and measurement errors. Experimental results are presented to show the effectiveness of the proposed scheme.

Keywords: 6 DOF manipulator; Joint-Task space; Robust tracking control; Fast friction estimation; Electrical cylinder.

1. INTRODUCTION

Parallel robot manipulators are widely used in entertainment and machine tool industries, due to its high power-to-weight ratios, great system stiffness, rapid responses and high accuracy (Chen [2013], Kim [2005]). However, the control of parallel electrical manipulator is challenging because of its highly nonlinear and complex dynamics, uncertain load disturbances and forward kinematics problem (Lebret [1993]). Some advanced control algorithms for parallel manipulator have been studied to achieve accurate trajectory tracking performance (Kim [2005], Chen [2013]). However, the feasibility of certain algorithm depends on the frameworks of the control scheme and what actuators are used in the parallel manipulator.

Parallel manipulator control scheme mainly stems from two frameworks: the task space control (Kim [2005], Davliakos [2008]) and the joint space control (Pi [2010]). The former is based on the dynamics described by the task space and needs the real-time states of the moving platform. This information can be obtained via costly direct measurements or state estimation methods such as forward kinematics. However, the 6-DOF sensors can definitely bring additional cost. Forward kinematics of 6-DOF parallel manipulator can be solved by numerical solution such as Newton-Raphson method with the information on actuator lengths (Parikh [2005]), but it can increase the calculation and communication burden of the computer. The joint space scheme is designed to make the actual actuator lengths track the desired lengths computed by an inverse kinematics. This control scheme is much simple as collection of multiple, independent single-input single-output(SISO) control systems using the information on each actuator length only (Pi [2010]). However, the controller design aiming for a high performance requires an almost accurate dynamic model of the parallel manipulator, even if some parameters are not fully known. Specially, a robust control scheme in the joint space has been proposed for parallel manipulator based on Lyapunov redesign method (Kim [2000]). Yet, the uncertainties are too conservative due to the inclusion of gravity and known dynamic characteristics. In this article, the control schemes handle the dynamics represented both in the joint space and in the task space.

On the other hand, the friction disturbances in electrical actuator systems cannot be neglected, and always impact on system performance greatly (Xu [2008], Lu [2009]). Furthermore, there are uncertainties in the friction properties, which depend on the load condition, due to electrical cylinders spiral drive way (Hao [2013]). Friction model-

⋆ This work was supported by National High Technology Researchand Development Program of China(863 Program, 2011AA041002)

ing and compensation have been studied extensively in other manipulator systems. Unfortunately, these friction observers are based on joint coordinates and cannot be directly applied to the parallel mechanism due to its highly coupled nonlinear dynamics. The Freidland-Park friction observer in the joint space coordinates has been used to provide friction estimates that help to improve the control performance for a 6-DOF parallel manipulator (Kim [2005]). Yet, the uncertainties in friction estimates are too conservative due to the conclusion of known equivalent load of each cylinder and the assumption that the parallel manipulator is an equivalent SISO system.

In this paper, the control schemes handle the dynamics represented both in the joint-task space by transforming the dynamics on the task space into joint space. The dynamic matrices are modeled as nominal value plus deviation. In order to reduce calculation amount and make the Jacobian valid, the desired positional data are used to calculate the nominal value. Thus the proposed scheme can manage the dynamics based on both on the joint space and task space, and the calculation amount is extremely minimized. In addition, an adaptation law based on Lyapunov design method is proposed to estimate the friction. To estimate the uncertain friction fast and effectively, the projection mapping, which has variable bounds, is designed to satisfy good robust performance. With the friction estimates available, the robust joint-task space control (RJTSC) scheme is proposed based on the Lyapunov design method to guarantee a practical stability under uncertainties such as inertia, modeling error, friction, and measurement errors. To test the proposed control scheme, RJTSC with fast friction estimator, robust joint space control (RJSC) and PID joint space control (PIDJSC) both with conservative friction estimator are compared by experimentation. The results show that the proposed RJTSC has a better performance.

The paper is organized as follows. The kinematics and dynamics of a 6-DOF manipulator are described in Section 2. Section 3 presents a fast friction estimation method and the proposed robust joint-task space control strategy and the accompanying stability analysis are addressed. Friction property identification method and experiments results are shown in Section 4.

2. SYSTEM MODEL

2.1 Dynamics of Electrical Cylinder

Each electrical cylinder consists of motor, nut and screw. The nut is driven by the motor through the electromagnetic torque transforming rotary motion into linear motion. The force transmissions inside the cylinder are shown in Fig.1. T_e, F_L respectively represent the electromagnetic torque and the load force. The force on the nut includes two parts: the friction f which is oriented along the movement and the normal force F_B which is perpendicular to the contact surface. Thus, the force equation is given by

$$\frac{2\pi T_e}{P} = F_L + \frac{\sqrt{\pi^2 D^2 + P^2}}{P} f. \tag{1}$$

where P, D respectively represent the lead and the diameter of the nut. Define the ith actuator force u_i as

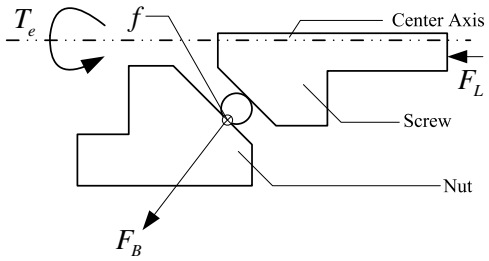

Fig. 1. Force transmissions inside the cylinder

$u_i = 2\pi T_e/P$ and the equivalent friction u_{fi} as $u_{fi} = \sqrt{\pi^2 D^2 + P^2} f/P$. In the following, $\mathbf{u} = [u_i]^T \in \mathbf{R}^6$ denotes the actuator forces vector, and $\mathbf{u_f} = [u_{fi}]^T \in \mathbf{R}^6$ is an equivalent friction vector for actuators and joints. In order to simplify the modeling problem, the following traditional static friction model is used:

$$\mathbf{F_f}(\dot{\mathbf{y}}) = \mathbf{sgn}(\dot{\mathbf{y}})\mathbf{F_c} + \dot{\mathbf{Y}}\mathbf{F_v}. \tag{2}$$

where $\dot{\mathbf{y}} = [\dot{y}_i]^T \in \mathbf{R}^6$ is the six link velocity vector. $\mathbf{F_f}(\dot{\mathbf{y}}) \in \mathbf{R}^6$ is the friction function vector which approximates the friction curve. $\mathbf{F_c} \in \mathbf{R}^6$ and $\mathbf{F_v} \in \mathbf{R}^6$ respectively represent the Coulomb friction coefficient and the viscous friction coefficient. The direction and velocity matrix are defined as $\mathbf{sgn}(\dot{\mathbf{y}}) = diag\{\mathrm{sgn}(\dot{y}_i)\} \in \mathbf{R^{6\times 6}}$ and $\dot{\mathbf{Y}} = diag\{\dot{y}_i\} \in \mathbf{R^{6\times 6}}$. With the friction model (2), the equivalent friction vector can be written as:

$$\mathbf{u_f}(\dot{\mathbf{y}}) = \mathbf{F_f}(\dot{\mathbf{y}}) - \mathbf{d_f}. \tag{3}$$

where $\mathbf{d_f}$ is the friction model approximation error vector. It should be stressed here that the friction coefficients $\mathbf{F_c}$ and $\mathbf{F_v}$ are time varying because the force perpendicular to the contact surface is changing with load force. Obviously, since the value and the changing rate of the load are all unknown, the friction coefficients need to be estimated as fast as possible.

2.2 Dynamics of Parallel Electrical Manipulator

The dynamics and kinematics of a 6-DOF parallel manipulator has been studied extensively. Hence, the dynamic model is briefly described in this paper. Fig.2 explains two coordinate systems: the $\{\mathbf{B}\}$ coordinate system is the inertial coordinate system, the $\{\mathbf{T}\}$ is the body coordinate system fixed to the top moving platform. The linear motions denoted as surge (q_1), sway (q_2), and heave (q_3) are along $\mathrm{X_B}-\mathrm{Y_B}-\mathrm{Z_B}$ axis for base coordinate system. The angular motions labeled as roll (q_4), pitch (q_5) and yaw (q_6) are $\mathrm{X_T}-\mathrm{Y_T}-\mathrm{Z_T}$ Euler angles. The body coordinate system $\{\mathbf{T}\}$ and the inertial coordinate system $\{\mathbf{B}\}$ are superimposed in the initial state $q_i = 0, i = 1, \cdots, 6$. The following dynamic model can be derived using the Euler-Lagrangian method:

$$\mathbf{M}(\mathbf{q},\sigma)\ddot{\mathbf{q}} + \mathbf{C}(\mathbf{q},\dot{\mathbf{q}},\sigma)\dot{\mathbf{q}} + \mathbf{G}(\mathbf{q},\sigma) = \mathbf{J}^T(\mathbf{q})(\mathbf{u} - \mathbf{u_f}). \tag{4}$$

where $\mathbf{M}(\cdot) \in \mathbf{R}^{6\times 6}$ is inertia, $\mathbf{C}(\cdot) \in \mathbf{R}^{6\times 6}$ is Coriolis and centrifugal force. $\mathbf{G}(\cdot) \in \mathbf{R}^6$ is gravitational force, and $\mathbf{J}(\cdot) \in \mathbf{R}^{6\times 6}$ is Jacobian. δ denotes uncertainties, and $\mathbf{q} = [q_i]^T \in \mathbf{R}^6$ is the displacement vector of the top moving platform. The dynamic model (4) is represented by the displacement vector $\mathbf{q}$. Furthermore, in Section 3, the

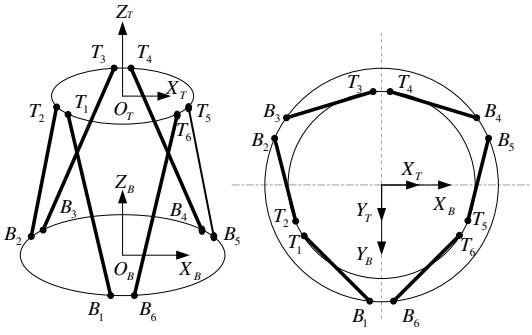

Fig. 2. Definition of coordinate systems for parallel manipulator

desired positional data are used to calculate the nominal, and the proposed control is designed to be robust to the uncertainties.

The dynamic equation on the joint space is derived from the following property by using the Jacobian matrix $\mathbf{J}(\cdot)$.

$$\dot{\mathbf{q}} = \mathbf{J}^{-1}(\mathbf{q})\dot{\mathbf{y}}. \tag{5}$$

Then the dynamic equation on the joint space can be constructed as:

$$\mathbf{M_1}(\mathbf{q},\sigma)\ddot{\mathbf{y}} + \mathbf{C_1}(\mathbf{q},\dot{\mathbf{q}},\sigma)\dot{\mathbf{y}} + \mathbf{G_1}(\mathbf{q},\sigma) = \mathbf{u} - \mathbf{u_f}. \tag{6}$$

where

$$\mathbf{M_1}(\mathbf{q},\sigma) = \mathbf{J}^{-T}(\mathbf{q})\mathbf{M}(\mathbf{q},\sigma)\mathbf{J}^{-1}(\mathbf{q}). \tag{7}$$

$$\mathbf{C_1}(\mathbf{q},\dot{\mathbf{q}},\sigma)=\mathbf{J}^{-T}(\mathbf{q})\mathbf{M}(\mathbf{q},\sigma)\dot{\mathbf{J}}^{-1}(\mathbf{q})+\mathbf{J}^{-T}(\mathbf{q})\mathbf{C}(\mathbf{q},\dot{\mathbf{q}},\sigma)\dot{\mathbf{J}}^{-1}(\mathbf{q}). \tag{8}$$

$$\mathbf{G_1}(\mathbf{q},\sigma) = \mathbf{J}^{-T}(\mathbf{q})\mathbf{G}(\mathbf{q},\sigma). \tag{9}$$

Two assumptions may be summarized as follows:

Assumption 1: The Jacobian is not singular.

Assumption 2: If σ represents uncertainties that include inertia, modeling error, and measurement noise, $\sigma \in \sum$, where $\sum$ is compact set.

In Lebret [1993], it can be proved that $\dot{\mathbf{M}} - 2\mathbf{C}$ satisfies the skew symmetric property. For the proof of the skew-symmetric property of $\dot{\mathbf{M}}_\mathbf{1} - 2\mathbf{C_1}$, the following Lemma is introduced which is adopted from Kim [2000].

Lemma 1: The matrix $\mathbf{M}$ and $\mathbf{M_1}$ are positive definite and symmetric. The $\dot{\mathbf{M}} - 2\mathbf{C}$ and $\dot{\mathbf{M}}_\mathbf{1} - 2\mathbf{C_1}$ satisfy skew-symmetric property, which means for any vector $\mathbf{x} \in R^6$, we have $\mathbf{x}^T(\dot{\mathbf{M}} - 2\mathbf{C})\mathbf{x} = 0$ and $\mathbf{x}^T(\dot{\mathbf{M}}_\mathbf{1} - 2\mathbf{C_1})\mathbf{x} = 0$.

3. FAST FRICTION ESTIMATION AND ROBUST CONTROL DESIGN

3.1 Fast Friction Estimation

Adaptive robust design based on Lyapunov method is used to construct the friction estimator. The key element of the adaptive robust design is to use the practical prior process information to construct projection type adaptation law for a controlled learning process even in the presence of disturbances. As in (Xu [2008]), the standard projection mapping is given to keep the parameter estimates within the known bounded set. Obviously, the bounds are prior known constants near the constant parameters. However, in electrical cylinder, the friction coefficients are time varying based on the load force. So the constant bounds must be chosen large enough to cover the extent of the varying function, this maybe lead to a slow estimation because of the large searching space. On the other hand, when the estimates diverge from the real value a lot, the adaption law should be redesigned to accelerate the estimating speed. Meanwhile, the robust performance should still be satisfied. Therefore, the projection type adaptation law should both be sensitive to bounds and have robust performance. To solve these problems, the projection mapping for time varying parameters is designed as:

$$proj_{\hat{\theta}}(\bullet) = \begin{cases} \bullet & \hat{\theta} \in \overset{\circ}{\Omega}_{\theta t} \ or \ n_{\hat{\theta}}^T \bullet \le 0 \\ (I - \Gamma \dfrac{n_{\hat{\theta}} n_{\hat{\theta}}^T}{n_{\hat{\theta}}^T \Gamma n_{\hat{\theta}}}) \bullet & \hat{\theta} \in \partial\Omega_{\theta\max} \ and \ n_{\hat{\theta}}^T \bullet > 0 \\ \bullet + \varepsilon \Gamma a & \hat{\theta} \in \breve{\Omega}_{\theta t} \end{cases} \tag{10}$$

where $\bullet \in R^n$ is any n-dimension vector and $\Gamma(t) \in \mathbf{R}^{n\times n}$ can be any time-varying positive definite symmetric matrix. In(10), $\overset{\circ}{\Omega}_{\theta t}$ and $\breve{\Omega}_{\theta t}$ denote the interior and the external of the set $\Omega_{\theta t}$ at time t separated by the time varying bound $\partial\Omega_{\theta t}$. $\partial\Omega_{\theta\max}$ denotes the maximum bound of $\Omega_{\theta t}$ independent of time t. In other words, the processing bound $\partial\Omega_{\theta t}$ of $\Omega_{\theta t}$ varies with t and the global bound $\partial\Omega_{\theta\max}$ is constant. We assume that the mapping between $\partial\Omega_{\theta t}$ and observable states can be prior designed according to the required performance. $n_{\hat{\theta}}$ represents the outward unit normal vector at $\hat{\theta} \in \partial\Omega_{\theta\max}$. ε is a positive real number and $a \in \mathbf{R}^n$ is a vector synthesized later. Throughout the article, $\hat{\theta}$ denotes the estimate of θ, and $\tilde{\theta}$ denotes the estimation error, which is defined by $\tilde{\theta} = \hat{\theta} - \theta$.

Lemma 2: Suppose that the parameter estimate $\hat{\theta}$ is updated using the following projection type adaptation law:

$$\dot{\hat{\theta}} = Proj_{\hat{\theta}}(\Gamma\tau). \tag{11}$$

where τ is the estimation function and $\Gamma = diag\{\tau_1, \tau_2, \cdots, \tau_n\} > 0$ is any continuously differentiable positive symmetric adaptation rate matrix. With this adaptation structure, the following desirable properties hold:

P1: The parameter estimates are always within the set Ω_θ with the known bound $\partial\Omega_{\theta\max}$.

P2: $\tilde{\theta}^T \left[\Gamma^{-1} Proj_{\hat{\theta}}(\Gamma\tau) - \tau\right] \le 0$

P3: For time varying parameters, if $\hat{\theta} \in \breve{\Omega}_{\theta t}$, $\exists\varepsilon \in \mathbf{R}, a \in \mathbf{R}^n$ such that $\hat{\theta}$ coverage to $\overset{\circ}{\Omega}_{\theta t}$.

Proof. Case1: If the parameters $\theta_i \in \theta$ are constant, make their bounds fixed to the maximum $\theta_{i\min}$ and $\theta_{i\max}$. Then according to (Xu [2008]), P1 and P2 can be verified.

Case2: And now we consider the parameters $\theta_j \in \theta$ are time-varying. P1 also holds because $\Omega_{\theta t}$ is a subset of Ω_θ. When $\hat{\theta}_j \in \overset{\circ}{\Omega}_{\theta t}$, P2 can be verified as in Case 1. And when the estimates lie out of $\Omega_{\theta t}$ i.e.$\hat{\theta}_j \in \breve{\Omega}_{\theta t}$, there will be a hyper plane strongly separating $\hat{\theta}_j$ and $\Omega_{\theta t}$. We denote this hyper plane as H_a^σ, where vector a is the normal of H_a^σ towards the side of $\Omega_{\theta t}$ and σ is defined as the inner product of a and any other vector x at the hyper plane,

i.e., $\langle a, x\rangle = \sigma$. And when $\hat{\theta}_j \in \breve{\Omega}_{\theta t}$ the real value θ_j and the estimated value $\hat{\theta}_j$ are separated by the hyper plane, then we have

$$\left\langle a, \hat{\theta}_j \right\rangle \leq \sigma \leq \langle a, \theta_j \rangle \Rightarrow \left\langle a, \tilde{\theta}_j \right\rangle \leq 0. \tag{12}$$

Considering the last line in (10), we have $\tilde{\theta}_j^T[\Gamma^{-1} Proj_{\hat{\theta}_j}(\Gamma\tau) - \tau] = \varepsilon\tilde{\theta}_j^T a \leq 0, \forall\tau$, which means P2 also holds. For vector a is the normal of H_a^σ towards the side of $\Omega_{\theta t}$ and ε is a positive real number without changing the direction of a, P3 holds.

As a result, the following bounds-varying projection type on-line adaptation laws are used to estimate the unknown friction coefficients:

$$\dot{\hat{\mathbf{F}}}_\mathbf{c} = Proj\{-(\dot{\mathbf{e}}+\mathbf{S_1 e})^T \mathbf{sgn}(\dot{\mathbf{y}})\mathbf{\Gamma_1}\}. \tag{13}$$

$$\dot{\hat{\mathbf{F}}}_\mathbf{v} = Proj\{-(\dot{\mathbf{e}}+\mathbf{S_1 e})^T \dot{\mathbf{Y}}\mathbf{\Gamma_2}\}. \tag{14}$$

where $\mathbf{\Gamma_1}, \mathbf{\Gamma_2} > 0 \in \mathbf{R^{6\times 6}}$ are diagonal matrices.

Remark 1: Here, we assume that the time varying bound $\partial\Omega_{\theta t}$ is known function of observable states. In practice, the load force can be estimated using the following method explained in remark 3. Therefore, using the load force estimate, $\partial\Omega_{\theta t}$ can be calculated by the mapping between $\partial\Omega_{\theta t}$ and the load force. The mapping is designed according to the experiments for friction characteristic identification in section 4.

3.2 Robust Tracking Control Law

The main focus of this subsection is to design a robust controller based on the joint-task space coordinates to guarantee a high tracking control performance in the presence of uncertainty. The control block diagrams for RJTSC strategy and another control schemes (RJSC, PIDJSC) are described in 3.The following assumptions 3 and 4 are made for the robust control design.

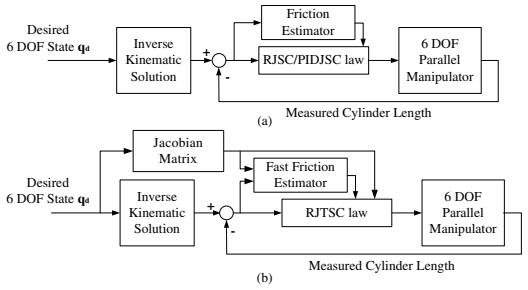

Fig. 3. Control block diagrams for (a) RJSC and PIDJSC (b) RJTSC

Assumption 3: There exist positive constants $\underline{\sigma}$ and $\bar{\sigma}$ such that

$$\underline{\sigma} \leq \mathbf{M_1}(\mathbf{q}, \sigma) \leq \bar{\sigma} \;\; \forall \mathbf{q} \in \mathbf{R}^6 \;\; \forall \sigma \in \sum. \tag{15}$$

Assumption 4: Each matrix in the dynamics (6) can be represented as nominal with deviation:

$$\mathbf{M_1}(\mathbf{q}, \sigma) = \mathbf{M_0}(\mathbf{q_d}, 0) + \delta\mathbf{M_1}(\mathbf{q}, \sigma). \tag{16}$$

$$\mathbf{C_1}(\mathbf{q}, \dot{\mathbf{q}}, \sigma) = \mathbf{C_0}(\mathbf{q_d}, \dot{\mathbf{q}}_\mathbf{d}, \sigma) + \delta\mathbf{C_1}(\mathbf{q}, \dot{\mathbf{q}}, \sigma). \tag{17}$$

$$\mathbf{G_1}(\mathbf{q}, \sigma) = \mathbf{G_0}(\mathbf{q_d}, 0) + \delta\mathbf{G_1}(\mathbf{q}, \sigma). \tag{18}$$

Remark 2: If the measurements or the estimates of the positional data $\mathbf{q}$ contain uncertainties, the control function with the inverse of $\mathbf{J}^T(\cdot)$ is no longer valid. In order to reduce calculation amount and make the Jacobian valid, the desired positional data $\mathbf{q_d}$ is used to calculate the nominal in Assumption 4. In actual operation, the difference between $\mathbf{q_d}$ and $\mathbf{q}$ is small and bounded, so it is possible to apply a MIMO robust control scheme. Later in Section 4, the experimental results show that the estimates are reasonable.

Remark 3: With the assumption 4 and the friction estimate, the load force can be estimated

$$\hat{\mathbf{F}}_\mathbf{L} = \mathbf{M_0}(\mathbf{q_d}, 0)\ddot{\mathbf{y}} + \mathbf{C_0}(\mathbf{q_d}, \dot{\mathbf{q}}_\mathbf{d}, 0)\dot{\mathbf{y}} + \mathbf{G_0}(\mathbf{q_d}, 0). \tag{19}$$

The load force estimate $\hat{\mathbf{F}}_\mathbf{L}$ is chosen to calculate the time varying bound $\partial\Omega_{\theta t}$ in Lemma 2.

Define the joint displacement tracking error $\mathbf{e} \in \mathbf{R}^6$ and its derivative $\dot{\mathbf{e}} \in \mathbf{R}^6$ as

$$\mathbf{e} = \mathbf{y} - \mathbf{y_d}, \quad \dot{\mathbf{e}} = \dot{\mathbf{y}} - \dot{\mathbf{y}}_\mathbf{d}. \tag{20}$$

where $\mathbf{y_d}$ represent the desired actuator displacement. Then, the system dynamics (6) with definition of joint displacement tracking error becomes

$$\begin{aligned}\mathbf{M_1}(\mathbf{q}, \sigma)\ddot{\mathbf{e}} + \mathbf{C_1}(\mathbf{q}, \dot{\mathbf{q}}, \sigma)\dot{\mathbf{e}} = &-\mathbf{M_0}(\mathbf{q_d}, 0)\ddot{\mathbf{y}}_\mathbf{d} - \mathbf{C_0}(\mathbf{q_d}, \dot{\mathbf{q}}_\mathbf{d}, 0)\dot{\mathbf{y}}_\mathbf{d} \\ &- \mathbf{G_0}(\mathbf{q_d}, 0) + \mathbf{u} - \mathbf{F_f}(\dot{\mathbf{y}}) + \mathbf{h_1}\end{aligned} \tag{21}$$

$$\mathbf{h_1}(\cdot) = -\delta\mathbf{M_1}(\mathbf{q}, \sigma)\ddot{\mathbf{y}}_\mathbf{d} - \delta\mathbf{C_1}(\mathbf{q}, \dot{\mathbf{q}}, \sigma)\dot{\mathbf{y}}_\mathbf{d} - \delta\mathbf{G_1}(\mathbf{q}, \sigma) + \mathbf{d_f}. \tag{22}$$

Theorem 1: Suppose that there exists a bounding function $\rho_1(\cdot)$ that satisfies condition (23). Then, the system (21) is practically stable if the control law (25) is applied with the assumptions 1-4.

$$\|\varphi(\cdot)\| \leq \rho_1(\cdot). \tag{23}$$

where

$$\varphi(\cdot) = \mathbf{h_1}(\cdot) + \delta\mathbf{M_1 S_1}\dot{\mathbf{e}} + \delta\mathbf{C_1 S_1 e}. \tag{24}$$

$$\mathbf{u} = \mathbf{u_1} + \mathbf{u_2}. \tag{25}$$

where

$$\begin{aligned}\mathbf{u_1} = &\mathbf{M_0}(\ddot{\mathbf{y}}_\mathbf{d} - \mathbf{S_1}\dot{\mathbf{e}}) + \mathbf{C_0}(\dot{\mathbf{y}}_\mathbf{d} - \mathbf{S_1 e}) \\ &+ \mathbf{G_0} + \mathbf{sgn}(\dot{\mathbf{y}})\hat{\mathbf{F}}_\mathbf{c} + \dot{\mathbf{Y}}\hat{\mathbf{F}}_\mathbf{v} - \mathbf{K_p e} - \mathbf{K_v}\dot{\mathbf{e}}\end{aligned}. \tag{26}$$

$$\mathbf{u_2} = \begin{cases} -\dfrac{\mathbf{w_1}}{\|\mathbf{w_1}\|}\rho_1(\cdot) & if\ \|\mathbf{w_1}\| \geq \varepsilon_1 \\ -\dfrac{\mathbf{w_1}}{\varepsilon_1}\rho_1(\cdot) & if\ \|\mathbf{w_1}\| < \varepsilon_1 \end{cases} \tag{27}$$

where $\mathbf{K_p}, \mathbf{K_v} \in \mathbf{R}^{6\times 6}$, $\mathbf{K_p}, \mathbf{K_v}$ are symmetric positive-definite matrices, $\mathbf{S_1} = diag(S_{1i}) \in \mathbf{R}^{6\times 6}$, $S_{1i} > 0$, $\mathbf{K_p} + \mathbf{S_1 K_v} > 0$, $\begin{bmatrix} \mathbf{K_p} & \mathbf{0} \\ \mathbf{0} & \mathbf{S_1 K_v} \end{bmatrix} > 0$, and $\mathbf{w_1}(\cdot) = (\dot{\mathbf{e}} + \mathbf{S_1 e})\rho_1(\cdot)$.

Proof. Define Lyapunov function candidate V_1 as

$$\begin{aligned}V_1 = &\frac{1}{2}(\dot{\mathbf{e}} + \mathbf{S_1 e})^T\mathbf{M_1}(\dot{\mathbf{e}} + \mathbf{S_1 e}) \\ &+ \frac{1}{2}\mathbf{e}^T(\mathbf{K_p} + \mathbf{S_1 K_v})\mathbf{e} + \frac{1}{2}\tilde{\mathbf{F}}_\mathbf{c}^\mathbf{T}\mathbf{\Gamma_1}\tilde{\mathbf{F}}_\mathbf{c} + \frac{1}{2}\tilde{\mathbf{F}}_\mathbf{v}^\mathbf{T}\mathbf{\Gamma_2}\tilde{\mathbf{F}}_\mathbf{v}.\end{aligned} \tag{28}$$

By assumption 3, the positive definitiveness and decrescent property of the first two terms of V_1 can be proved identical to the one in Kim [2005]. Considering $\mathbf{\Gamma_1}, \mathbf{\Gamma_2} > 0 \in \mathbf{R^{6\times 6}}$,

the quadratic form $\frac{1}{2}\tilde{\mathbf{F}}_\mathbf{c}^\mathbf{T}\mathbf{\Gamma_1}\tilde{\mathbf{F}}_\mathbf{c}$ and $\frac{1}{2}\tilde{\mathbf{F}}_\mathbf{v}^\mathbf{T}\mathbf{\Gamma_2}\tilde{\mathbf{F}}_\mathbf{v}$ are non-negative and decrescent as

$$\lambda_{\min}(\mathbf{\Gamma_1},\mathbf{\Gamma_2})||\tilde{\mathbf{F}}||^2 \leq \frac{1}{2}\tilde{\mathbf{F}}_\mathbf{c}^\mathbf{T}\mathbf{\Gamma_1}\tilde{\mathbf{F}}_\mathbf{c}+\frac{1}{2}\tilde{\mathbf{F}}_\mathbf{v}^\mathbf{T}\mathbf{\Gamma_2}\tilde{\mathbf{F}}_\mathbf{v} \leq \lambda_{\max}(\mathbf{\Gamma_1},\mathbf{\Gamma_2})||\tilde{\mathbf{F}}||^2. \quad (29)$$

where $\tilde{\mathbf{F}} = [\tilde{\mathbf{F}}_\mathbf{c}, \tilde{\mathbf{F}}_\mathbf{v}]^T$. By Lemma 2, the estimates error vector $\tilde{\mathbf{F}}$ is bounded as

$$0 \leq ||\tilde{\mathbf{F}}||^2 \leq ||\tilde{\mathbf{F}}_{\mathbf{c}\max}||^2 + ||\tilde{\mathbf{F}}_{\mathbf{v}\max}||^2 = ||\tilde{\mathbf{F}}||^2_{\max} \quad (30)$$

Therefore, V_1 is positive definite and decrescent as

$$\tau_1||\mathbf{z_1}||^2 \leq V_1 \leq \tau_2||\mathbf{z_1}||^2 + ||\tilde{\mathbf{F}}||^2_{\max} \quad (31)$$

where $\mathbf{z_1} = [\mathbf{e}, \dot{\mathbf{e}}]^T$, and the positive coefficients τ_1, τ_2 are identical to those in Kim [2005].The derivative of V_1 along the trajectory of the system (21) is given by

$$\begin{aligned}\dot{V}_1 = &(\dot{\mathbf{e}}+\mathbf{S_1}\mathbf{e})^T\mathbf{M_1}(\ddot{\mathbf{e}}+\mathbf{S_1}\dot{\mathbf{e}}) + (\dot{\mathbf{e}}+\mathbf{S_1}\mathbf{e})^T\dot{\mathbf{M}}_\mathbf{1}(\dot{\mathbf{e}}+\mathbf{S_1}\mathbf{e}) \\ &+ \mathbf{e}^T(\mathbf{K_p}+\mathbf{S_1}\mathbf{K_v})\dot{\mathbf{e}} + \dot{\hat{\mathbf{F}}}_\mathbf{c}^\mathbf{T}\mathbf{\Gamma}_\mathbf{1}^{-1}\tilde{\mathbf{F}}_\mathbf{c} + \dot{\hat{\mathbf{F}}}_\mathbf{v}^\mathbf{T}\mathbf{\Gamma}_\mathbf{2}^{-1}\tilde{\mathbf{F}}_\mathbf{v}\end{aligned} \quad (32)$$

According to (13), (14), (25) the skew-symmetric property on $\dot{\mathbf{M}}_\mathbf{1} - 2\mathbf{C_1}$ shown in Lemma 1, and properties of projection type shown in Lemma 2, it can be seen that

$$\begin{aligned}\dot{V}_1 = &(\dot{\mathbf{e}}+\mathbf{S_1}\mathbf{e})^T(\mathbf{u_2}+\mathbf{h_1}+\delta\mathbf{C_1}\mathbf{S_1}\mathbf{e}+\delta\mathbf{M_1}\mathbf{S_1}\dot{\mathbf{e}}) - \mathbf{e}^T\mathbf{S_1}\mathbf{K_p}\mathbf{e} - \dot{\mathbf{e}}^T\mathbf{K_v}\dot{\mathbf{e}} \\ &+\left[\dot{\hat{\mathbf{F}}}_\mathbf{c}^\mathbf{T}\mathbf{\Gamma}_\mathbf{1}^{-1}+(\dot{\mathbf{e}}+\mathbf{S_1}\mathbf{e})^T\mathbf{sgn}(\dot{\mathbf{y}})\right]\tilde{\mathbf{F}}_\mathbf{c} + \left[\dot{\hat{\mathbf{F}}}_\mathbf{v}^\mathbf{T}\mathbf{\Gamma}_\mathbf{2}^{-1}+(\dot{\mathbf{e}}+\mathbf{S_1}\mathbf{e})^T\dot{\mathbf{Y}}\right]\tilde{\mathbf{F}}_\mathbf{v} \\ &\leq (\dot{\mathbf{e}}+\mathbf{S_1}\mathbf{e})^T(\mathbf{u_2}+\varphi) - \lambda_{\min}(\mathbf{S_1}\mathbf{K_p},\mathbf{K_v})(||\mathbf{e}||^2+||\dot{\mathbf{e}}||^2)\end{aligned} \quad (33)$$

The rest of the proof is identical to the one in Kim [2005], and it can be proved that if $\|\mathbf{w_1}\| \geq \varepsilon_1$ the first term in (33) becomes

$$(\dot{\mathbf{e}}+\mathbf{S_1}\mathbf{e})^T(\mathbf{u_2}+\varphi) \leq 0 \quad (34)$$

If $\|\mathbf{w_1}\| < \varepsilon_1$, those become from (27)

$$(\dot{\mathbf{e}}+\mathbf{S_1}\mathbf{e})^T(\mathbf{u_2}+\varphi) \leq \frac{\varepsilon_1}{4} \quad (35)$$

Therefore, $\dot{V}_1$ is bounded by

$$\dot{V}_1 \leq \frac{\varepsilon_1}{4} - \lambda_{\min}(\mathbf{S_1}\mathbf{K_p},\mathbf{K_v})(||\mathbf{e}||^2+||\dot{\mathbf{e}}||^2) = -\eta_1||\mathbf{z_1}||^2 + \frac{\varepsilon_1}{4} \quad (36)$$

where $\eta_1 := \lambda_{\min}(\mathbf{S_1}\mathbf{K_p},\mathbf{K_v})$. Thus, $\dot{V}_1 < 0$ for all $\|\mathbf{z_1}\| > \sqrt{\frac{\varepsilon_1}{4\eta_1}} = R_z$. Following (36), we can satisfy the requirements of the practical stability with uniform stability (ball size of R_z).

4. EXPERIMENT

4.1 Friction Property Identification

To identify the friction property, the loading system for single electrical cylinder is setup as shown in Fig.4. The electrical cylinder is placed vertically and connected to the platform with ball joint. The electrical cylinder is controlled by the Kollmorgen motor driver in constant velocity motions. During the motion, the friction can be indirectly measured by the difference between the output force of the motor and the gravity of the weights. The experiments have been conducted with different weights and different velocities. Then the off-line friction curve is carried out as Fig.5, in which the proposed dynamic fiction model simplified to (2) neglecting low speed condition. From friction curve, we get the nominal value of the

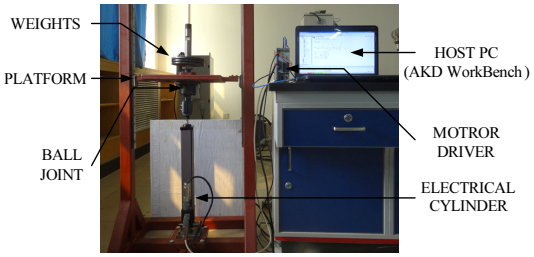

Fig. 4. The loading system for single electrical cylinder

friction parameters $F_c = (94 + 0.204F_L)/N$, and $F_v = 142.8N \cdot s/m$. The estimation parameters are $\mathbf{\Gamma_1} = 0.5 \cdot \mathbf{I}$, and $\mathbf{\Gamma_2} = 10 \cdot \mathbf{I}$. With remark 3, the time varying bound $\partial\Omega_{\theta t}$ is chosen as $[94 + 0.19\hat{\mathbf{F}}_\mathbf{L}, 94 + 0.22\hat{\mathbf{F}}_\mathbf{L}]$.

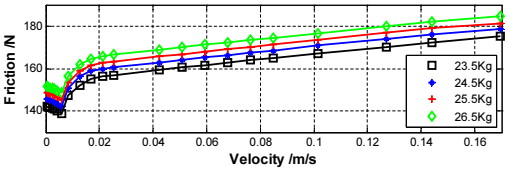

Fig. 5. The off-line friction curve with weigts 23.5-26.5Kg

4.2 System Setup

The control performance of the proposed RJTSC is evaluated on a 6-DOF parallel manipulator in Fig.6 via experiments, which features monitor interface (PC-based system), control unit (resolving CPU, control CPU and amplifier) and six electrical cylinders. The control time for the system is 1.57ms. The parameters of the parallel manipulator are summarized in Table 1.

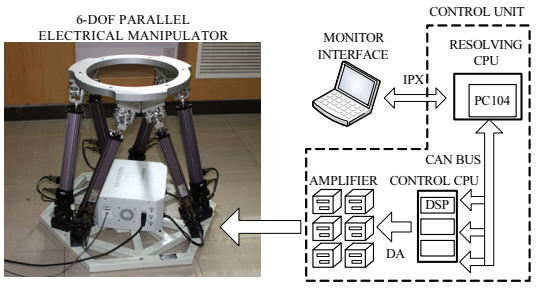

Fig. 6. Control system for a 6-DOF parallel manipulator

Table 1. Parameters of parallel manipulator

Parameter	Description	Value	Unit
$l_{min}l_{max}$	Min/Max. Length	0.65/0.95	m
m	Mass of Top	25.0	Kg
$I_{xx}I_{yy}I_{zz}$	Inertia of Top	0.45,0.49,0.71	Kgm^2
R_BR_T	Radius of Bottom/Top	0.35/0.24	m

The off-line forward kinematic solution is used to estimate the 6 DOF states. The measured cylinder lengths are compared to the inverse kinematic solution based on the estimates from the off-line Newton-Raphson numerical method.The results show less than $0.001mm^2$, which confirms that the tracking errors can be defined as the difference between the desired states and the off-line estimates in the following subsection.

4.3 Comparative Experimental Results

The performance of the proposed RJTSC with fast friction estimator is presented in this subsection through the dynamic friction model and off-line estimates of 6-DOF states obtained in the previous subsections. RJSC and PIDJSC both with conservative friction estimator are applied as fair benchmarking controllers. The PIDJSC gains Kp, Ki, Kd are experimentally tuned to be 100, 10, and 5, respectively. The control gains for the RJTSC and RJSC are $\mathbf{K_p} = 1.5 \cdot \mathbf{I}$, $\mathbf{K_v} = 0.1 \cdot \mathbf{I}$, $\mathbf{S_1} = 10 \cdot \mathbf{I}$ and $\varepsilon_1 = 2.0$. Although the RJTSC gains seem much smaller than those of PIDJSC, it should be noted that the RJTSC calculates the desired force from the nominal gain matrices, while the PIDJSC produces just control input to the position error. Fig.10-11 show tracking errors under sinu-

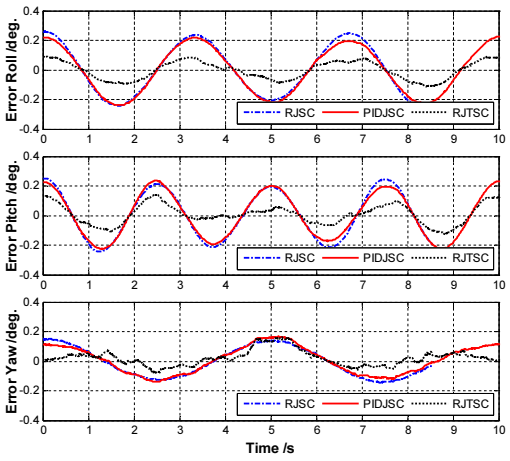

Fig. 7. The rotational tracking errors

soidal inputs along six directions: roll ($7.0°/0.3Hz$), pitch ($5.0°/0.4Hz$), yaw ($6.0°/0.2Hz$), surge (0.05m/0.2Hz), sway (0.05m/0.3Hz), heave (0.04m/0.2Hz) motions. As shown in these figures, the tracking errors of the RJSC and PIDJSC appear periodical trend with inputs and have the rotational error bounds within $\pm 0.3°$ and translation error bounds within $\pm$2mm. By contrast, the rotational error bounds of the RJTSC are bounded within $\pm 0.1°$ and the translation error bounds are bounded below $\pm$0.7mm. The excellent control performance by the RJTSC stems from its joint-task based designs and fast friction estimation. In other words, the RJTSC cancels the nonlinearities including the inertia force for a given acceleration, the gravitational force, the Coriolis and centrifugal forces and uncertain frictions.

5. CONCLUSION

This paper studies the robust tracking control problem of a 6-DOF electrical parallel manipulator. A robust control algorithm on the proposed joint-task space frameworks is designed. With such a control structre, the model accuracy can be guaranteed and the calculation amount is reduced simultaneously. By using prior knowlege of friction property related to the load condition, a fast friction estimator is presented to estimate the uncertain friction due to electrical cylinders spiral drive way. Friction property identification and comparative experiments are carried out and the

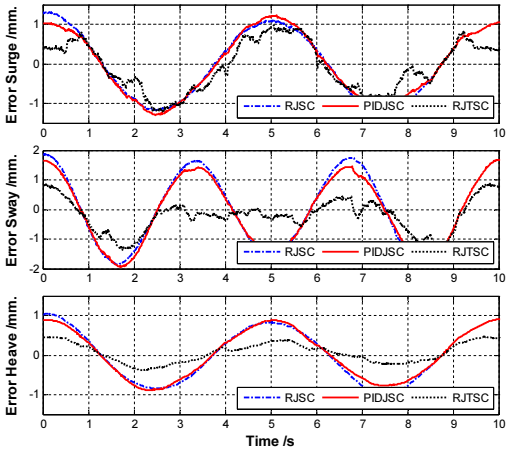

Fig. 8. The translation tracking errors

performance demonstrate the effectiveness of the proposed approach. The proposed methodology can be applied in almost all parallel systems with uncertain frictions.

REFERENCES

Chen, S.H., Fu, L.C. Output feedback sliding mode control for a stewart platform with a nonlinear observer-based forward kinematics solution. *IEEE Trans. on Control Systems Technology*, vol. 21, no. 1, pp. 176-185, 2013.

Davliakos, I., & Papadopoulos, E. Model-based control of a 6-dof electrohydraulic Stewart-Gough platform. *Mechanism and Machine Theory*, vol. 43, no. 11, pp. 1385-1400, 2008.

Hao, R.J., Wang, J.Z., & Zhao, J.B. Adaptive robust control for electric linear actuator using modified LuGre model with fast load-based parameter estimation. *Proc. of the 32nd Chinese Control Conference*, pp. 412-417, Xian'an, China, 2013.

Kim, D.H., Kang, J.Y., & Lee, K. Robust Tracking Control Design for a 6 DOF Parallel Manipulator. *Jounal of Robotic Systems*, vol. 17, no. 10, pp. 527-547, 2000.

Kim, H.S., Cho, Y.M., & Lee, K. Robust nonlinear task space control for 6 DOF parallel manipulator. *Automatica*, vol. 41, no. 9, pp. 1591-1600, 2005.

Lebret, G., Liu, K., & Lewis, F.L. Dynamic analysis and control of a stewart platform manipulator. *Jounal of Robotic Systems*, vol. 10, no. 5, pp. 629-655, 1993.

Lu, L., Yao, B., Wang, Q.F., & Chen, Z. Adaptive robust control of linear motors with dynamic friction compensation using modified LuGre model. *Automatica*, vol. 45, no. 12, pp. 2890-2896, 2009.

Parikh, P.J., & Lam, S.S.Y. A hybrid strategy to solve the forward kinematics problem in parallel manipulators. *IEEE Trans. on Robotics*, vol. 21, no. 1, pp. 18-25, 2005.

Pi, Y.J., & Wang, X.Y. Observer-based cascade control of a 6-DOF parallel hydraulic manipulator in joint space coordinate. *Mechatronics*, vol. 20, no. 6, pp. 648-655, 2010.

Xu, L., & Yao, B. Adaptive robust control of mechanical systems with non-linear dynamic friction compensation. *International Journal of Control*, vol. 81, no. 2, pp. 167-176, 2008.